CANADIAN APPLIED
MATHEMATICS QUARTERLY
Volume 21, Number 3, Fall 2013

KELVIN-HELMHOLTZ INSTABILITY OF A BOTTOM-INTENSIFIED JET IN A STRATIFIED-FLUID

CHANDANA R. SOMAYAJI AND GORDON E. SWATERS

ABSTRACT. Kelvin-Helmholtz instability is the inertial destabilization of a parallel shear flow in a density stratified fluid under the influence of gravity. For example, this type of instability manifests itself as surface waves in the ocean when wind blows over the water surface. In this paper we solve the nonhydrostatic Kelvin-Helmholtz instability problem for a near-bottom jet with a continuous velocity profile in a flat-bottomed nonrotating density-stratified fluid. Of particular note, the nonhydrostatic stability problem modelled here has a high wavenumber cutoff and does not exhibit an ultraviolet catastrophe unlike other inviscid stability calculations that have been previously published.

1 Introduction The fundamental problem in the study of the stability of parallel flows is to determine whether a given shear flow is stable to traveling wave perturbations or not [**10**]. Since the work of Helmholtz [**6**] and Kelvin [**8**] on the stability of homogeneous and stratified vortex sheets in the 19th century, numerous authors have examined increasingly complex problems in an attempt to understand the basic properties associated with the transition to instability of fluid flows.

Rayleigh [**12**] examined a piecewise-linear representation of the homogeneous shear layer and performed a stability analysis on this idealized shear layer. The results produced are in qualitative agreement with subsequent studies of smooth profiles, such as the hyperbolic tangent shear layer (see, for example, [**3**]). This suggests that in treating the stability of shear layers it is very useful to study piecewise-linear shear layers in order to capture the basic instability mechanism ([**2, 11**]). Holmboe [**7**], motivated by geophysical flows, extended Rayleigh's analysis to include a stable density stratification, retaining the piecewise-linear shear layer and including a layered piecewise-constant density profile. These ideal-

ized profiles give qualitatively similar results to the smooth profiles, as in the homogeneous case [**5**].

In the context of this paper, Swaters [**16**] investigated the stability characteristics of overflows that were nonrotating and baroclinic, and where it was possible for both frictionally induced and Kelvin-Helmholtz instability to occur. A two-layered shallow-water model was used, resulting in the Kelvin-Helmholtz instability being hydrostatic. In the inviscid limit, the linear stability analysis of the two-layered shallow-water equations lead to an ultraviolet catastrophe [**10**]. Since this is not a desirable part of the model, we attempt a step toward gaining a better understanding of the instability in the nonhydrostatic case, where, in most cases, the most unstable mode is located at a finite wavenumber and there exists a high wavenumber cutoff.

During the course of this work, we first examined in some detail, the stability characteristics of a piecewise linear homogeneous shear layer flow [**14**]. This enabled us to obtain certain general physical properties from the dispersion relation obtained and some analytical and computational techniques which were used in the main analysis of the non homogeneous flow profile described in this paper.

The paper is organized as follows. Section 2 introduces the model geometry and the equations governing the model; the linear stability problem is then used to obtain the Taylor-Goldstein equation. In Section 3, we perform the normal mode stability analysis and solve the normal mode equations using the appropriate jump conditions across the interfaces to obtain the non dimensional dispersion relation after introducing the nondimensionalization parameters. We then consider some special limits of the dispersion relation in Section 4. The Marginal Stability Boundary (MSB) and its characteristics are determined in Section 5. For a more complete analysis of the MSB, we determine the stability characteristics of the MSB one parameter at a time in Section 6. Section 7 summarizes the paper and states some limitations and scope for future research.

2 Governing equations The geometry of the three-layered model we are considering is shown in Figure 1. The depth of the entire water column is H, η_1 and η_2 are the nondimensional disturbances in the middle and lower layer thicknesses, respectively, compared to the scale thickness and h_0 and d are the mean layer depths for the middle and lower layers, respectively. The stratification and velocity profiles depicted in Figure 1 emulate real world observations of bottom intensified

abyssal overflows (Swaters, personal communication). We will assume a density profile given by

$$\rho_H = \begin{cases} \rho_1, & d \le z \le H, \\ \rho_2, & 0 \le z \le d. \end{cases}$$

The background flow is assumed to be piecewise continuous and linear, given by,

$$U(z) = \begin{cases} 0, & h_0 \le z \le H, \\ \dfrac{U_0(z-h_0)}{d-h_0}, & d \le z \le h_0, \\ \dfrac{U_0 z}{d}, & 0 \le z \le d. \end{cases}$$

This profile is a model for a boundary jet located immediately adjacent to the bottom where the velocity is continuous but not differentiable and the maximum velocity is located at $z = d$ and the minimum jet velocity ($U_0(z) = 0$) is located at $z = h_0$ in the flow interior. As shown in Figure 1, the interval $h_0 < z < H$ will be defined as region I, $d < z < h_0$ will be defined as region II and $0 < z < d$ will be defined as region III.

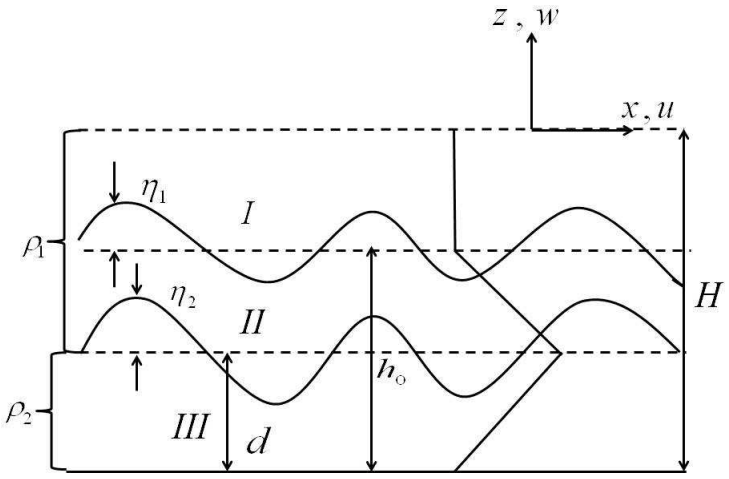

FIGURE 1: The geometry of the model

The inviscid, incompressible and stratified 2-D flow is governed by the set of partial differential equations [**9**]:

$$\rho(\partial_t + u\partial_x + w\partial_z)u + p_x = 0, \tag{1}$$

$$\rho(\partial_t + u\partial_x + w\partial_z)w + p_z = -\rho g, \tag{2}$$

$$(\partial_t + u\partial_x + w\partial_z)\rho = 0, \tag{3}$$

$$u_x + w_z = 0, \tag{4}$$

where u and w are the velocities in the positive x and z directions, respectively, p is the total pressure field, ρ is the variable density, g is the acceleration due to gravity and t is the time. Equations (1) and (2) represent the conservation of horizontal and vertical momentum, respectively. Equation (3) represents incompressibility and equation (4) represents conservation of mass.

It is possible to show that $u = U_0(z)$, $w = 0$, $p = p_H(z)$ and $\rho = \rho_H(z)$ where $p_H(z)$ and $\rho_H(z)$ are the hydrostatic pressure and the hydrostatic density fields, respectively, is an exact steady state solution of the equations of motion for any smooth function $U_0(z)$. We try to examine the linear stability of this exact solution. Thus, we now add perturbations to the exact solutions of the form

$$u(x, z, t) = U_0(z) + \tilde{u}(x, z, t), \tag{5}$$

$$w(x, z, t) = 0 + \tilde{w}(x, z, t), \tag{6}$$

$$\rho(x, z, t) = \rho_H(z) + \tilde{\rho}(x, z, t), \tag{7}$$

$$p(x, z, t) = p_H(z) + \tilde{p}(x, z, t), \tag{8}$$

where the tildes represent perturbation quantities. Substituting equations (5), (6), (7) and (8) into our model equations (1), (2), (3) and (4), neglecting nonlinear perturbation terms, dropping the tildes on the perturbation quantities and invoking the Boussinesq approximation ([**9**]), we get

$$\rho_\star(\partial_t + U_0(z)\partial_x)u + \rho_\star w U_0' = -p_x, \tag{9}$$

$$\rho_\star(\partial_t + U_0(z)\partial_x)w = -p_z - \rho g, \tag{10}$$

$$(\partial_t + U_0\partial_x)\rho + w\rho_{H\,z} = 0, \tag{11}$$

$$u_x + w_z = 0. \tag{12}$$

where

$$\rho_\star = \frac{1}{H}\int_0^H \rho_H(z)\,dz.$$

Equations (9), (10), (11) and (12) are called the Linear Stability Equations (LSE) and $U_0' \equiv dU_0(z)/dz$. Equations (9) and (10) are the perturbation momentum equations in the x and z direction respectively, (11) is the perturbation density equation and (12) is the perturbation continuity equation.

Introducing the normal modes into the LSE,

$$(u, w, \rho, p) = (u'(z), w'(z), \rho'(z), p'(z))\exp[ik(x - ct)] + \text{c.c.}, \tag{13}$$

where the primes here denote the normal mode amplitude functions. Dropping the primes and eliminating p' and ρ in the normal mode equations, we obtain the Boussinesq Taylor-Goldstein (TG) equation given by

$$[\rho_\star(U_0 - c)w']' - [\rho_\star U_0' w]' - \left[\frac{\rho_H' g}{U_0 - c} + \rho_\star k^2(U_0 - c)\right] w = 0. \tag{14}$$

3 Normal mode stability analysis The continuity equation (12) enables us introduce the stream function, $\phi(x, z, t)$ such that $u = -\phi_z$ and $w = \phi_x$ [**4**]. We now use the normal mode representation

$$\phi = \varphi(z)\exp[ik(x - ct)] + \text{c.c.},$$

which implies

$$u = -\varphi' \tag{15}$$

and

$$w = ik\varphi. \tag{16}$$

Therefore, substituting (16) into the TG equation (14), we get

$$[\rho_\star(U_0 - c)\varphi']' - [\rho_\star U_0'\varphi]' - \left[\frac{\rho_H' g}{U_0 - c} + \rho_\star k^2(U_0 - c)\right] \varphi = 0. \tag{17}$$

Since the flow profile is linear (i.e., $U_0'' \equiv 0$, except across the interfaces), the TG equation reduces to simply

$$\varphi'' - k^2\varphi = 0$$

in all three regions.

We will solve the reduced TG equation in each region and then match the solutions across the interfaces where U_0', U_0'' and ρ_H' are not defined, both at $z = h_0$ and $z = d$, respectively, using appropriate jump conditions. The solutions for ϕ in the three regions can be written in the form

$$\varphi_I(z) = A\sinh[k(H - z)], \tag{18}$$

$$\varphi_{II}(z) = B\sinh[k(z - d)] + D\sinh[k(h_0 - z)], \tag{19}$$

and

$$\varphi_{III}(z) = E\sinh[kz], \tag{20}$$

which satisfy the rigid-lid and bottom boundary condition $w = 0$ at $z = 0$ and $z = H$. The first condition we impose is the kinematic condition, which states that fluid particles on the interface must move with the interface without the two fluids occupying the same point at the same time and without a cavity forming between the fluids [**10**]. This condition across both $z = h_0$ and $z = d$ translates to

$$[\phi] = 0, \tag{21}$$

where the jump is defined as

$$[\star] \equiv \star^+ - \star^-. \tag{22}$$

The second matching condition we need is the dynamic condition which postulates that the normal component of the stress vector at the deforming interface is continuous [**10**]. Across the $z = h_0$ interface, this implies

$$[(U_0 - c)\phi' - U_0'\phi] = 0, \tag{23}$$

where the square brackets indicate the jump defined by (22).

The pressure continuity condition across $z = d$, where the density is discontinuous, is given by

$$\left[\rho_\star(U_0 - c)\phi' - \rho_\star U_0'\phi - \frac{\rho_H g\phi}{U_0 - c}\right] = 0, \tag{24}$$

where the square brackets indicate the jump defined by (22).

Applying the kinematic and pressure continuity conditions to the solutions (18), (19) and (20) across the interfaces $z = h_0$ and $z = d$, respectively, and demanding that the determinant of the coefficients of the thusly obtained equations vanishes in order to have nontrivial solutions for A and E, we get the following cubic dispersion relation [**14**],

$$
\begin{aligned}
&c^3k^2\sinh[kH] + c^2U_0\left[\frac{kh_0}{d(h_0-d)}\sinh[k(H-d)]\sinh[kd]\right.\\
&\quad\left.-\frac{k}{h_0-d}\sinh[kh_0]\sinh[k(H-h_0)] - 2k^2\sinh[kH]\right]\\
&\quad + cU_0^2\left[k^2\sinh[kH]\right.\\
&\quad -\frac{h_0}{d(h_0-d)^2}\sinh[kd]\sinh[k(H-h_0)]\sinh[k(h_0-d)]\\
&\quad -\frac{kh_0}{d(h_0-d)}\sinh[kd]\sinh[k(H-d)]\\
&\quad +\frac{2k}{h_0-d}\sinh[kh_0]\sinh[k(H-h_0)]\\
&\quad \left.-\frac{g'k}{U_0^2}\sinh[kd]\sinh[k(H-d)]\right]\\
&\quad +\left[\frac{g'U_0}{h_0-d}\sinh[k(H-h_0)]\sinh[k(h_0-d)]\sinh[kd]\right.\\
&\quad +\frac{U_0^3h_0}{d(h_0-d)^2}\sinh[kd]\sinh[k(H-h_0)]\sinh[k(h_0-d)]\\
&\quad \left.-\frac{U_0^3k}{h_0-d}\sinh[k(H-h_0)]\right] = 0.
\end{aligned}
$$

This equation forms the dispersion relation for the instability problems where we consider c as a function of U_0, k, h_0, d and g', i.e., $c = c(U_0, k, h_0, d, g')$.

We now introduce the following nondimensionalization in order to

simplify the dispersion relation,

$$\tilde{k} = kH,$$
$$\tilde{d} = \frac{d}{H},$$
$$\tilde{h}_0 = \frac{h_0}{H},$$
$$\tilde{c} = \frac{c}{\sqrt{gH}},$$

where the tildes denote nondimensional quantities.

Substituting the nondimensional parameters into the dimensional dispersion relation, dropping tildes and dividing by $[gH]^{3/2}/H^2$, we get the nondimensional dispersion relation

$$\begin{aligned}(25)\quad & c^3k^2\sinh[k] + c^2F\left[\frac{kh_0}{d(h_0-d)}\sinh[k(1-d)]\sinh[kd] - 2k^2\sinh[k]\right.\\ & \left. - \frac{k}{h_0-d}\sinh[kh_0]\sinh[k(1-h_0)]\right]\\ & + c\left[F^2\left\{\frac{2k}{h_0-d}\sinh[kh_0]\sinh[k(1-h_0)]\right.\right.\\ & - \frac{h_0}{d(h_0-d)^2}\sinh[kd]\sinh[k(1-h_0)]\sinh[k(h_0-d)]\\ & \left.\left. - \frac{kh_0}{d(h_0-d)}\sinh[kd]\sinh[k(1-d)] + k^2\sinh[k]\right\}\right.\\ & \left. - \delta k\sinh[kd]\sinh[k(1-d)]\right]\\ & + \left[F\delta\frac{1}{(h_0-d)}\sinh[k(1-h_0)]\sinh[k(h_0-d)]\sinh[kd]\right.\\ & + F^3\sinh[k(1-h_0)]\left\{\frac{h_0}{d(h_0-d)^2}\sinh[kd]\sinh[k(h_0-d)]\right.\\ & \left.\left. - \frac{k}{h_0-d}\sinh[kh_0]\right\}\right] = 0,\end{aligned}$$

where the Froude number, $F \equiv U_0/\sqrt{gH}$ and the scaled reduced gravity is $\delta \equiv g'/g$.

4 Special limits/analysis of the dispersion relation We now consider some special limits applied to the nondimensional dispersion relation (25).

1. $F = 0$: The first limit we consider is the no mean flow limit, i.e., $U_0 = 0$. This means the Froude number, $F \equiv U_0/\sqrt{gH} = 0$. Substituting $F = 0$ in (25) gives

$$c^3k^2 \sinh[k] - c\delta k \sinh[kd] \sinh[k(1-d)] = 0,$$

which reduces to

$$c = \pm\sqrt{\frac{\delta \sinh[kd] \sinh[k(1-d)]}{k \sinh[k]}}.$$

From the above formulation, the flow is stable if and only if $\rho_2 > \rho_1$, i.e., for a stable density stratification ($\delta > 0$). The propagating waves are simply neutral internal gravity waves in a two-layered fluid [**9**].

2. $\delta = 0$: Setting $\delta = 0$ reduces the non dimensional dispersion relation (25) to the homogenous limit since $\delta = 0 \implies \rho_2 = \rho_1$. Substituting $\delta = 0$ in the nondimensional dispersion relation (25) yields, after a little algebra

$$\begin{aligned}(26)\qquad & k^2 \sinh[k](c^3 + cF^2 - 2Fc^2) \\ & + \frac{kh_0}{d(h_0-d)} \sinh[k(1-d)] \sinh[kd](c^2F - cF^2) \\ & + \frac{k}{h_0-d} \sinh[kh_0] \sinh[k(1-h_0)](2cF^2 - c^2F - F^3) \\ & + \frac{h_0}{d(h_0-d)^2} \sinh[kd] \sinh[k(1-h_0)] \\ & \times \sinh[k(h_0-d)](F^3 - cF^2) = 0.\end{aligned}$$

We can factor out $(c - F)$ in the above equation, which reduces the equation to the nondimensional dispersion relation obtained in the ho-

mogeneous case ([**14**]),

$$
\begin{aligned}
(27)\qquad c^2k^2\sinh[k] + cF\Bigg[&\frac{k}{d(h_0-d)}\{h_0\sinh[k(1-d)]\sinh[kd] \\
&- d\sinh[k(1-h_0)]\sinh[kh_0]\} - k^2\sinh[k]\Bigg] \\
&+ \frac{F^2\sinh[k(1-h_0)]}{d(h_0-d)^2}(-h_0\sinh[k(h_0-d)]\sinh[kd] \\
&+ kd(h_0-d)\sinh[kh_0]) = 0,
\end{aligned}
$$

where the Froude number, $F \equiv U_0/\sqrt{gH}$.

The above dispersion relation can be written in the form

$$
c^2 + cF\alpha + F^2\beta = 0, \tag{28}
$$

where

$$
\begin{aligned}
\alpha \equiv \frac{k}{k^2 d(h_0-d)\sinh[k]}&(\{h_0\sinh[k(1-d)]\sinh[kd] \\
&- d\sinh[k(1-h_0)]\sinh[kh_0]\} - k^2\sinh[k]),
\end{aligned}
$$

and

$$
\begin{aligned}
\beta \equiv \frac{\sinh[k(1-h_0)]}{k^2 d(h_0-d)^2\sinh[k]}&\big\{kd(h_0-d)\sinh[kh_0] \\
&- h_0\sinh[k(h_0-d)]\sinh[kd]\big\}.
\end{aligned}
$$

The solutions for equation (28) are given by the quadratic formula,

$$
c = \frac{-\alpha F \pm F\sqrt{\alpha^2 - 4\beta}}{2}.
$$

Instability occurs when the discriminant, $\alpha^2 - 4\beta < 0$. The instability corresponds to the Rayleigh destabilization of a vortex sheet in a homogeneous fluid [**4**]. As we are primarily interested in the Kelvin-Helmholtz instability when $\rho_2 \neq \rho_1$, we do not provide the analysis for this case here, but all details can be found in [**14**].

5 Marginal stability boundary In order to determine the MSB, we first rewrite the cubic nondimensional dispersion relation (25) in the form

$$\begin{aligned}(c-F)\Bigg[&c(c-F)k^2\sinh[k]+cF\frac{kh_0}{d(h_0-d)^2}\sinh[k(1-d)]\sinh[kd]\\&-F(c-F)\frac{k}{h_0-d}\sinh[kh_0]\sinh[k(1-h_0)]\\&-F^2\frac{h_0}{d(h_0-d)^2}\sinh[kd]\sinh[k(1-h_0)]\Bigg]\\&+\delta\Bigg[\frac{F}{h_0-d}\sinh[k(1-h_0)]\sinh[k(h_0-d)]\sinh[kd]\\&-ck\sinh[k(1-d)]\sinh[kd]\Bigg]=0,\end{aligned}$$

which can be written as

$$(c-F)(c^2a+cFb+F^2d)+\delta(cM+\gamma F)=0, \tag{29}$$

where

$$\begin{aligned}a&=k^2\sinh[k],\\b&=\left(\frac{kh_0}{d(h_0-d)}\sinh[k(1-d)]\sinh[kd]\right.\\&\qquad\left.-\frac{k}{h_0-d}\sinh[kh_0]\sinh[k(1-h_0)]\right)-k^2\sinh[k],\\d&=\frac{k}{h_0-d}\sinh[kh]\sinh[k(1-h_0)]\\&\qquad-\frac{h_0}{d(h_0-d)^2}\sinh[kd]\sinh[k(1-h_0)],\\M&=-k\sinh[k(1-d)]\sinh[kd],\\\gamma&=\frac{1}{h_0-d}\sinh[k(1-h_0)]\sinh[k(h_0-d)]\sinh[kd].\end{aligned}$$

Rewriting (29) in the form,

$$c^3a+c^2F(b-a)+cF^2(d-b)-F^3d=0,$$

and assuming $c = \tilde{c}F$, the above equation reduces to ([**1**]),

$$\tilde{c}^3 a + \tilde{c}^2(b-a) + \tilde{c}\left[(d-b) + \frac{\delta M}{F^2}\right] + \left[\frac{\delta\gamma}{F^2} - d\right] = 0.$$

Following the general procedure to solve a cubic equation, we let $\tilde{c} = t - \frac{b-a}{a}$ to get an equation in terms of t,

$$t^3 + pt + q = 0, \tag{30}$$

where p and q are defined by [**1**],

$$p = \frac{3a[(d-b) + \frac{\delta M}{F^2}] - (b - a^2)}{3a^2},$$
$$q = \frac{2(b-a)^3 - 9a(b-a)[(d-b) + \frac{\delta M}{F^2}] + 27a^2[\frac{\delta\gamma}{F^2} - d]}{27a^3}.$$

The roots of the cubic (30) will all be real (and hence the flow will be stable) when,

$$\tau \equiv -\frac{q^2}{4} - \frac{p^3}{27} \geq 0, \tag{31}$$

where τ is a function of $k,\ h_0,\ d,\ \delta$ and F. Instability occurs when $\tau < 0$ (i.e., when there are complex roots to (30)) and the marginal stability boundary is obtained when $\tau \equiv 0$. The parameter surface for which,

$$\tau(k, h_0, d, \delta, F) = 0,$$

is a multidimensional hyper surface in 5-dimensional space. Therefore, it is easiest to visualize the transition from stability to instability one parameter at a time.

As an example of the transition to instability, we plot, in Figure 2, τ vs k, assuming $h_0 = 0.5,\ d = 0.25,\ F = 0.013$ and $\delta = 10^{-4}$. From Figure 2 we see that in the region $3.257 \approx k_l < k < k_u \approx 12.14$, $\tau < 0$ and therefore, the flow is unstable in this region. The points of marginal stability, i.e., the marginal stability boundaries, are at $k = k_l \approx 3.257$ and $k = k_u \approx 12.14$, where k_l is the low wavenumber cutoff and k_u is the high wavenumber cut-off.

From the estimates from Swaters [**16**], where $H \approx 800$ m, $U_0 = 1$ ms^{-1} and $g' \approx 7.2 \times 10^{-4}$ m $^{-2}$, the dimensional upper wavenumber

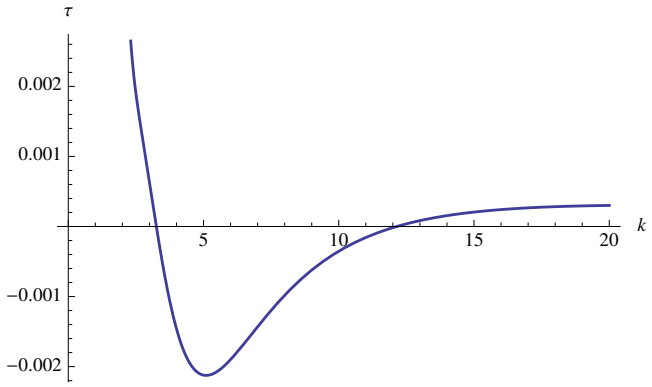

FIGURE 2: τ vs. k for $0 \leq k \leq 20$ with $h_0 = 0.5$, $d = 0.25$, $\delta = 10^{-4}$ and $F = 0.013$. The points of marginal stability are located at $k \approx 3.257$ and $k \approx 12.14$.

cutoff is about 0.015 m^{-1}, with the corresponding dimensional wavelength about 418.88 m. Similarly, the dimensional lower wavenumber cutoff is found to be about 0.004 m^{-1} and the corresponding dimensional wavelength about 1.57 km.

The dimensional phase velocity, $c_R = \mathrm{Re}\,(c)$ corresponding to the lower wavenumber cutoff, k_l is approximately 0.0144 ms^{-1} and that corresponding to the high wavenumber cutoff, k_u is about 0.0089 ms^{-1}.

The dimensional frequency, ω, which is given by

$$\omega = c_R k,$$

where c_R and k represent the dimensional phase velocity and wavenumber, respectively. The frequency corresponding to the low wavenumber cutoff is about 5.76×10^{-5} s^{-1} and that corresponding to the high wavenumber cutoff is approximately 1.335×10^{-4} s^{-1}.

The period of oscillation, T, given by

$$T = \frac{2\pi}{\omega},$$

associated with the low wavenumber cutoff is $T_l = 30.3$ hours, and that corresponding to the high wavenumber cutoff is $T_u = 13$ hours.

The graphs of the frequency and the phase velocity vs. k when $h_0 = 0.5$ and $d = 0.25$ are depicted in Figures 3 and 4, respectively.

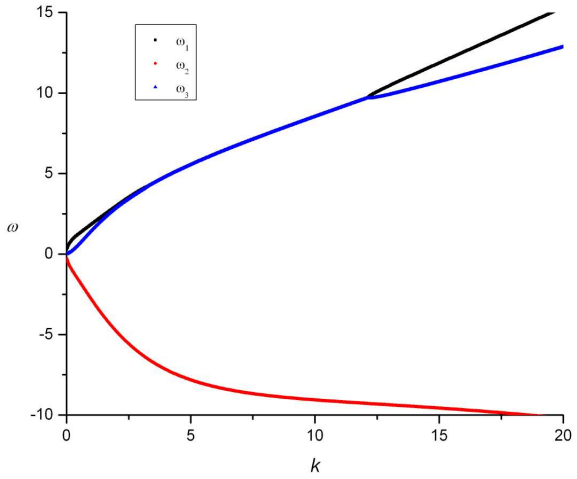

FIGURE 3: Graph of the nondimensional frequency, ω, when $h_0 = 0.5$, $d = 0.25$, $\delta = 10^{-4}$ and $F = 0.013$.

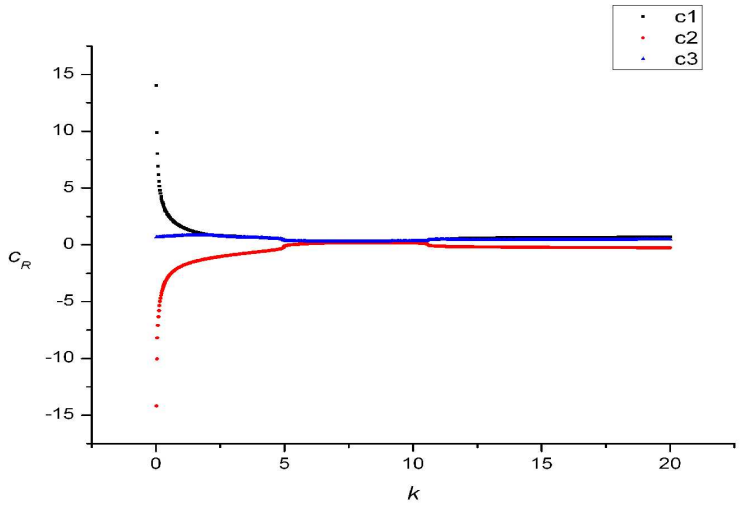

FIGURE 4: Graph of the nondimensional phase velocity, c_R, when $h_0 = 0.5$, $d = 0.25$, $\delta = 10^{-4}$ and $F = 0.013$.

In Figure 3, ω_1 and ω_3 coalesce when the flow is unstable, and ω_2 represents the root that is real. Similarly, in Figure 4, c_1 and c_2 coalesce

at the region of instability, with c_2 always being 'real'.

The graph of the growth rate, σ, vs. k is shown in Figure 5. We deduce from the figure, that between the regions $k_l \approx 3.257$ and $k_u \approx 12.14$, $\tau < 0$ which implies instability in that region.

The dimensional growth rate is given by

$$\sigma^\star = \frac{\sigma}{T},$$

where T represents the time scale (found to be 9.03 s). For $h_0 = 0.5$, $d = 0.25$, $\delta = 0.0001$ and $F = 0.013$, the growth rate of the most unstable mode, $\sigma_{\max}$ is about 0.329. This translates to a dimensional value of 0.0365 s $^{-1}$, which corresponds to a rapid e-folding amplification time of 27.39 s.

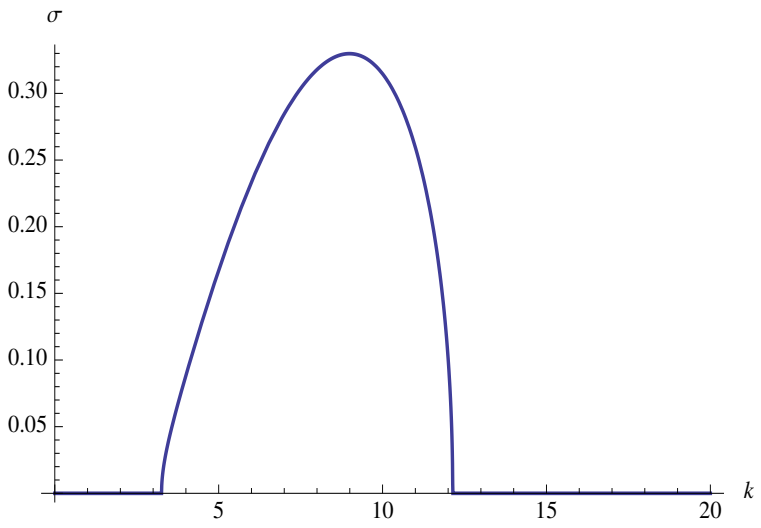

FIGURE 5: Growth rate curve for $h_0 = 0.5$, $d = 0.25$, $\delta = 10^{-4}$ and $F = 0.013$.

6 Stability diagrams In this section, we present a series of contour plots describing the instability characteristics when some of the parameters are varied. The upper and lower wavenumber cutoffs are determined by setting

$$\tau(k, h_0, d, \delta, F) = 0, \tag{32}$$

and solving for k as a function of h_0 and d, with δ and F being constants. We first choose $\delta = 10^{-5}$ and $F = 0.013$. The solutions of (32) were obtained numerically using Mathematica. We note here again that d is always less than h_0 as can be deduced from the geometry of the model (1). The contour plots of k_l and k_u, respectively, for the region of h_0 and d given by $0 < h_0 < 1$ and $d < h_0 < 1$, are presented in Figures 6 and 7, respectively.

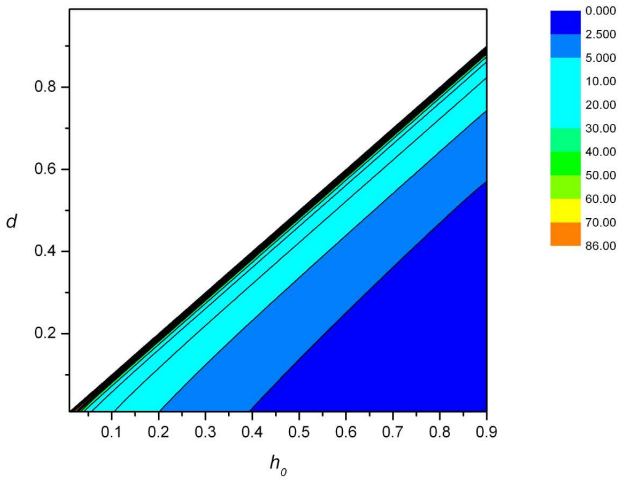

FIGURE 6: The k_l contours for varying h_0 and d with $\delta = 10^{-5}$ and $F = 0.013$.

To better understand the behaviour of the lower and upper wave numbers, we plot k_l vs. d and k_u vs. d for $h_0 = 0.5$, $\delta = 10^{-4}$ and $F = 0.013$. Since $d < h_0$ (Figure 1), $d < 0.5$. From Figure 8 we notice the lower wavenumber k_l has a slow but steady increase until $d \approx 0.4$ and 'blows up' around $d \approx 0.5$. The upper wavenumber k_u, has an initial

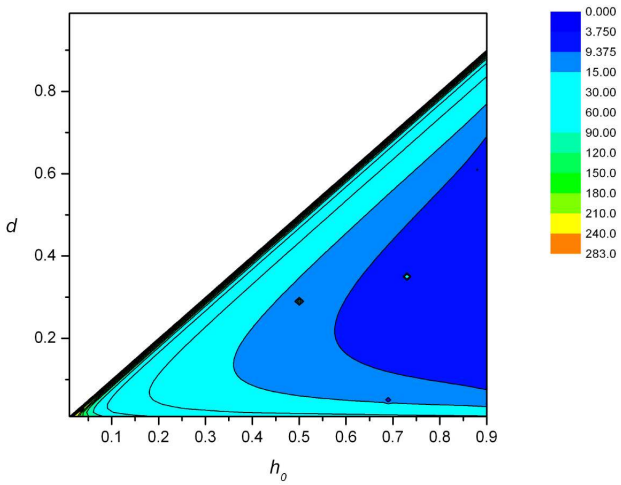

FIGURE 7: The k_u contours for varying h_0 and d with $\delta = 10^{-5}$ and $F = 0.013$.

decrease up to $d \approx 0.05$, plateaus until $d \approx 0.4$ and has a sharp increase thereafter as $d \to 0.5$. (See Figure 9.)

For $\delta = 10^{-5}$, $F = 0.013$ and $d = 0.25$, we plot k_l and k_u against h_0 in Figures 10 and 11, respectively, where $0 \leq h_0 \leq 1$. The lower wavenumber decreases for increasing h_0. Along the $d = 0.25$ contour, we notice a sharp decline in k_l around $h_0 = 0.3$, and as $h_0 \to 1$, k_l tends to 0. This can be inferred from the contour plots in Figures 6 and 7.

We can do a similar sort of analysis for the growth rate, wavenumber, frequency and phase velocity of the most unstable modes [**14**].

7 Effects of stratification In order to understand the effect of stratification on the instability of the flow, we plot the growth rate of the most unstable mode, $\sigma_{\max}$ against δ, the stratification parameter. We recall here that $\delta = g'/g$ with $g' = (\rho_2 - \rho_1)g/\rho$ where $\rho = (\rho_1 + \rho_2)/2$ is the average density.

In Figure 12, we plot $\sigma_{\max}$ vs. δ for $h_0 = 0.5$, $d = 0.25$ and $F = 1.5$, i.e., for a supercritical flow. The numerical computation was done using Mathematica. The x-axis representing δ goes from 10^{-4} to 10^{-2}, with increasing stratification. We notice that the growth rate of the most unstable mode decreases with increasing δ, which indicates that stratification has a stabilizing effect.

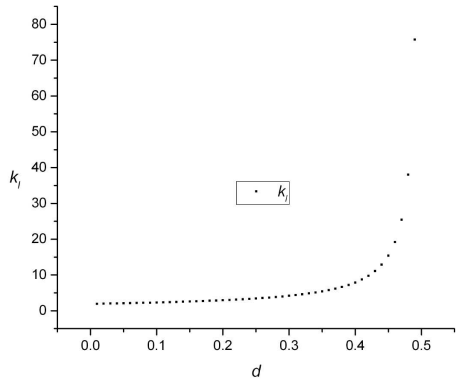

FIGURE 8: k_l for $h_0 = 0.5$ and varying d, with $\delta = 10^{-5}$ and $F = 0.013$.

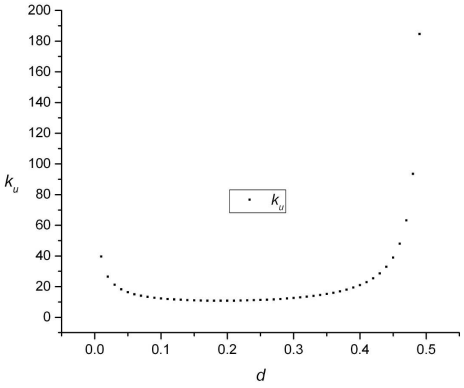

FIGURE 9: k_u for $h_0 = 0.5$ and varying d, with $\delta = 10^{-5}$ and $F = 0.013$.

With $F = 0.013$, δ again going from 10^{-4} to 10^{-2}, $h_0 = 0.5$ and $d = 0.25$, we plot $\sigma_{\max}$ vs. δ in Figure 13. We note that up to $\delta \approx 0.004$, stratification has a stabilizing effect. With a stronger stratification, $\delta > 0.004$, the stratification has a destabilizing effect. This is of course, an anomaly and is counterintuitive. However, if δ is increased beyond 10^{-2}, as is done in Figure 14, we notice the growth rate of the most unstable mode, $\sigma_{\max}$ starts to decrease around $\delta = 0.12$, which is indicative of a stabilizing effect with increasing stratification.

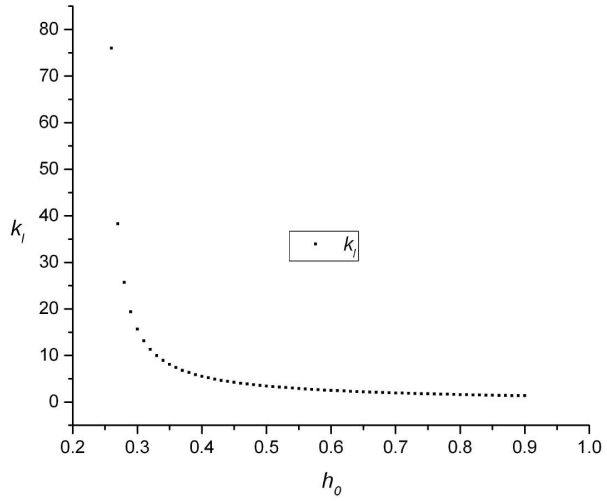

FIGURE 10: k_l for $d = 0.25$ and varying h_0, with $\delta = 10^{-5}$ and $F = 0.013$.

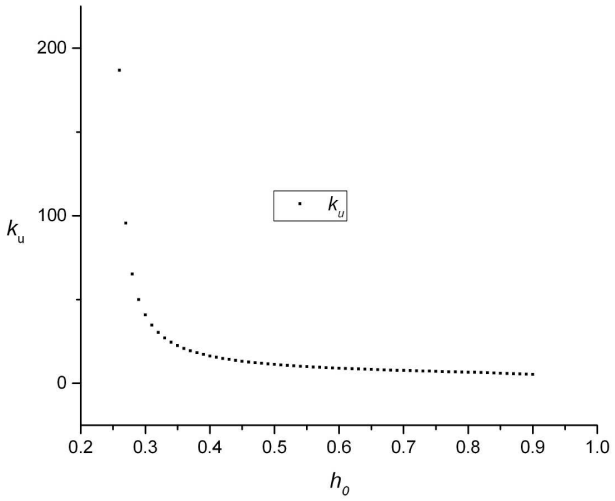

FIGURE 11: k_u for $d = 0.25$ and varying h_0, with $\delta = 10^{-5}$ and $F = 0.013$.

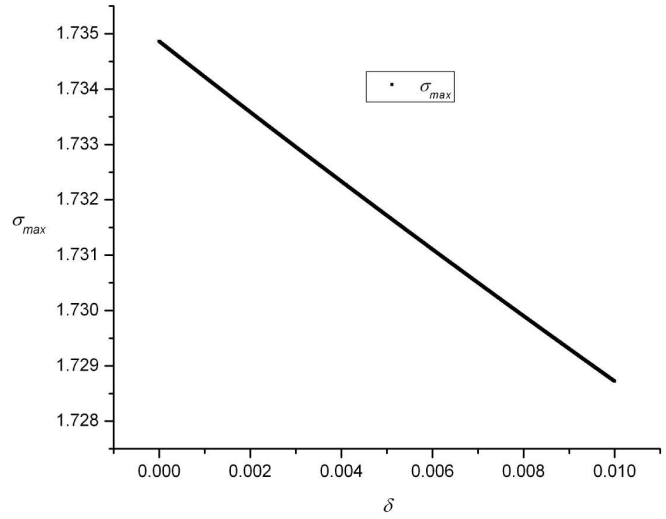

FIGURE 12: $\sigma_{\max}$ vs δ for $h_0 = 0.5,\ d = 0.25$ and $F = 1.5$.

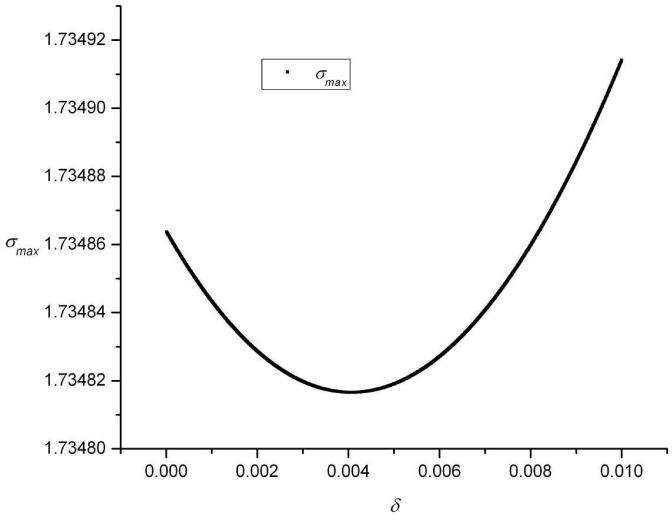

FIGURE 13: $\sigma_{\max}$ vs δ for $h_0 = 0.5,\ d = 0.25$ and $F = 0.013$.

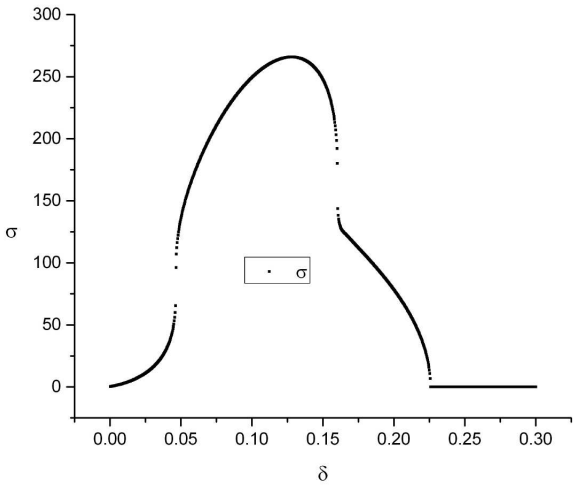

FIGURE 14: $\sigma_{\max}$ vs δ for $h_0 = 0.5,\ d = 0.25$ and $F = 0.013$.

8 Conclusion Based on the Swaters model in [**16**], in this paper, we have attempted a step toward gaining a better understanding of the shear layer Kelvin-Helmholtz instability in the nonhydrostatic case. We first introduced the equations governing the model and performed a linear stability analysis of the problem to then derive the Taylor Goldstein equation. After having obtained the normal mode equations, we stated the jump conditions across the interfaces that were then reconciled with the solutions of the model equations. The dispersion relation was then arrived at and the stability characteristics determined after performing a detailed analysis of the dispersion relation.

The mathematical and physical problem formulated and studied in this paper warrants further analysis. We found the dispersion relation for the non homogeneous flow more complex than the homogeneous one for performing any sort of asymptotic analysis. A more detailed investigation of the cubic dispersion relation would possibly help explain the counterintuitive result obtained in studying the effect of stratification on the stabilization of the flow, where we had a stronger stratification leading to destabilization in the case of δ, the stratification parameter, increasing from 10^{-4} to 10^{-2}.

Introducing rotation in the model equations would be another possible next step in further examining the Kelvin-Helmholtz instability of the

shear flow. In order to comply with the real world, most models employ a sloping topography (see, for example, [**13**], [**15**], [**16**], etc.). Therefore, investigating our problem on a sloping bottom would help us better understand the instability mechanism. Friction has also been a part of the models used in [**15**] and [**16**], so including friction in the fully nonlinear model equations would render the model more realistic. And finally, considering the limitations of linear stability theory, one could explore the solutions obtained in the weakly nonlinear case and also perhaps, the fully nonlinear equations, to obtain a more accurate picture of the transition to instability.

Acknowledgements This work was partially supported by Discovery Grant awarded by the Natural Sciences and Engineering Research Council to Gordon E. Swaters.

REFERENCES

1. Milton Abramowitz and Ireane A. Stegun, *Handbook of Mathematical Functions*, Dover Publications, 1964.
2. J. R. Carpenter, N. J. Balmforth and G. A. Lawrence, *Identifying unstable modes in stratifed shear layers*, Phys. Fluids **22** (2010), 054104.
3. P. G. Drazin, *The stability of a shear layer in an unbounded heterogeneous inviscid fluid*, J. Fluid Mech. **4** (1958), 214–224.
4. P. G. Drazin and W. H. Reid, *Hydrodynamic Stability*, Cambridge University Press, 1981.
5. Philip Hazel, *Numerical studies of the stability of inviscid stratifed shear flows*, J. Fluid Mech. **51** (1972), 39–61.
6. H. Helmholtz, *On the discontinuous movements of fluids*, Edinburgh Dublin Philos. Mag. J. Sci. **36** (1868), 337.
7. J. Holmboe, *On the behaviour of symmetric waves in stratified shear layers*, Geofysiske Publikasjoner **24** (1962), 67–113.
8. W. Kelvin, *Hydrokinetic solutions and observations*, Edinburgh Dublin Philos. Mag. J. Sci., **42** (1871), 362.
9. Pijush K. Kundu and Ira M. Cohen, *Fluid Mechanics*, Elsevier Inc., 2004.
10. Paul H. LeBlond and Lawrence A. Mysak, *Waves in the Ocean*, Elsevier Scientific Publishing Company, 1978.
11. Thomas P. Ray, *The effects of a simple shear layer on the growth of Kelvin-Helmholtz instabilities*, Mon. N. Roy. Astr. Soc. **198** (1982), 617–625.
12. J. W. S. Rayleigh, *On the stability, or instability, of certain fluid motions*, Proc. Lond. Math. Soc. **12** (1880), 57–72.
13. Mateusz K. Reszka, Gordon E. Swaters and Bruce R. Sutherland, *Instability of abyssal currents in a continuously stratified ocean with bottom topography*, J. Phys. Oceanogr. **32** (2002), 3528–3550.
14. Chandana Somayaji, *Kelvin-Helmholtz instabilitiy of a bottom intensified jet*, Master's thesis, University of Alberta, 2013.

15. Gordon E. Swaters, *Baroclinic characteristics of frictionally destabilized abyssal overflows*, J. Fluid Mech. **489** (2003), 349–379.
16. Gordon E. Swaters, *Mixed bottom-friction-Kelvin-Helmholtz destabilization of source-driven abyssal overflows in the ocean*, J. Fluid Mech. **626** (2009), 33–66.

Corresponding Author: Gordon E. Swaters
Department of Mathematical and Statistical Sciences,
University of Alberta, Edmonton, AB T6G 2G1
E-mail address: gswaters@ualberta.ca

Chandana R. Somayaji
Department of Mathematical and Statistical Sciences,
University of Alberta, Edmonton, AB T6G 2G1
E-mail address: csomayaj@ualberta.ca